Mixed multiscale finite elements and streamline methods for reservoir simulation of large geomodels [★]

Jørg E. Aarnes [a] Vegard Kippe [a] Knut–Andreas Lie [a,*]

[a] SINTEF ICT, Applied Mathematics, P.O. Box 124 Blindern, N–0314 Oslo, Norway

Abstract

We present a new approach to reservoir simulation that gives accurate resolution of both large-scale and fine-scale flow patterns. The method uses a mixed multiscale finite-element method (MMsFEM) to solve the pressure equation on a coarse grid and a streamline-based technique to solve the fluid transport on a fine-scale subgrid. The MMsFEM is based on the construction of special approximation velocity spaces that are adaptive to the local properties of the differential operator. As such, MMsFEM produces a detailed subgrid velocity field that reflects the impact of the fine-scale heterogeneous structures. By combining MMsFEM with rapid streamline simulation of the fluid transport, we aim towards a numerical scheme that facilitates routine reservoir simulation of large heterogeneous geomodels without upscaling. The new method is applied to two different test cases. The first test case consists of two (strongly) heterogeneous quarter five-spot problems in 2D. The second test case is a 3D upscaling benchmark taken from the 10th SPE Comparative Solution Project, a project whose purpose is to compare and validate upscaling techniques. The test cases demonstrate that the combination of multiscale methods and streamlines is a robust and viable alternative to traditional upscaling-based reservoir simulation.

Key words: reservoir simulation, multiscale methods, streamlines, upscaling
1991 MSC: 65M55, 65M60, 76S05

1 Introduction

The flow of displaced fluids in petroleum reservoirs is governed by processes and parameters occurring on multiple scales. A major challenge in reservoir simulation is therefore to represent and resolve all pertinent scales in both parameters and solution. In fact, the accuracy of reservoir simulation is largely controlled by the underlying geological grid models that give the geometry of the reservoir and specify rock parameters like porosity and permeability. Currently, the typical size of geomodels used for reservoir description exceeds by several orders of magnitude the capabilities of conventional reservoir simulators. State-of-the-art reservoir characterisation based on stochastic methods now allow geologists to generate a large number of plausible high-resolution grid models, each consisting of several million grid cells. Similarly, representing large-scale structures like channels and faults or complex trajectories of deviated, multi-branch wells requires complex gridding schemes like Voronoi (PEBI) grids, corner-point-grids, locally refined grids, flow-based grids, etc. Conventional simulator models are limited in size due to limitations in computational power, in particular, when multiple simulations are required as part of history matching, uncertainty assessment, and process optimisation. All three require fast and accurate flow simulations on a large number of plausible geological models on a routine basis, meaning that a single simulation should ideally run within seconds or minutes and not within hours or days.

The traditional approach to overcome the problem of scales is to use upscaling techniques to reduce the level of detail in the model parameters by carefully constructing coarser geomodels, where the number of geophysical parameters is reduced to a suitable size so that simulations can run within an acceptable time-frame. In other words, one uses some kind of averaging procedure to change the scale of the data. Alternatively, one can try to use the fine-scale description directly and incorporate it in the coarser simulation model through some kind of numerical subgrid technique.

In this paper we will follow the second approach and develop a new numerical scheme for incompressible, immiscible two-phase flow. The key idea is to use a mixed multiscale finite-element method [1] to discretise pressure and velocities and streamlines to discretise fluid transport. We believe that this combination can bring the art of reservoir simulation a big step towards routine simulation of high-resolution geomodels, possibly even on desktop computers. Indeed, this particular method allows the pressure equation to be solved on a coarse grid, and preserves important fine-scale features. Moreover, it produces velocity fields that are mass conservative on a subgrid scale so that we can use rapid streamline methods to compute the phase transport on a finer scale. Similar, but simpler and less rigorous ideas were presented earlier by Gautier et al. [2], who proposed an approximate multiscale method called nested gridding for

the pressure equation and a streamline method for the fluid transport on the fine scale.

Streamline methods are gaining in popularity and already provide desktop simulation of medium-sized reservoir models. Traditionally, streamline simulators have been based upon simplified physics, but recent advances have demonstrated the potential for more complex physics like compressible three-phase or component models [3,4]. A major obstacle in applying streamline methods to large geomodels is the need for *accurate* and *efficient* solution of the pressure equation. In particular, the pressure solver must be locally (and globally) mass-conservative and should handle strongly heterogeneous and anisotropic formations as well as irregular grids that conform to geological structures and complex well trajectories. Mixed finite-element methods (MFEM) and multi-point flux-approximation finite-volume methods (MPFA) [5–7] are examples of methods that handle these properties, and cover the most widely used methods for elliptic problems where mass preservation is an issue.

The first method that was labelled MsFEM was introduced by Hou and Wu [8]. This method is based on the construction of special finite-element base functions that are adaptive to the local property of the differential operator, and was introduced as a tool to solve elliptic partial differential equations with multiple-scale solutions. Although, MsFEM generates solutions that reflect the important fine-scale characteristics of the elliptic coefficients, these solutions are not locally mass conserving. By introducing a mixed MsFEM (MMsFEM), Chen and Hou [9] developed a multiscale method that is locally mass conserving on the *coarse* grid. Aarnes [1] extended the method further and developed a modified variant of MMsFEM that generates locally mass conservative velocity fields also on the subgrid scale. Local mass conservation is essential for a streamline method, and in the following we will therefore use Aarnes' modified method. Distinctly different, but related approaches include the multiscale finite-volume method by Jenny, Lee and Tchelepi [10], the nested-gridding method by Gautier, Blunt and Christie, and various numerical subgrid methods (see e.g., the overview by Arbogast [11] and references therein).

Although the current motivation for using MMsFEMs is increased computational speed, the improved flexibility may prove to be even more important for real fields with complex flow physics and irregular grids. MMsFEMs can easily handle grid blocks of arbitrary shape and are not confined to polygonal elements as is the case for ordinary finite-element methods. Moreover, the multiscale framework provides an ideal foundation for adaptive numerical schemes for phase-transport equations. This is because small-scale details in the velocity field only have a strong impact on the evolution of the saturation profile in the vicinity of the propagating saturation front. Thus, since the

subgrid velocity field provided by MMsFEM can be recovered from independent base functions, the subgrid information can easily be brought into action whenever it is needed in the simulation.

The main objective of the paper is to indicate that the combination of multiscale pressure solvers and streamline methods has a potential for direct simulation of high-resolution geomodels. We shall focus on computational accuracy, and will demonstrate that this multiscale-streamline approach is a robust and viable alternative to traditional upscaling-based reservoir simulation schemes. We show numerical results obtained on two heterogeneous quarter five-spot problems in 2D and on a medium-sized 3D model consisting of around 1,2 million grid cells from the 10th SPE Comparative Solution Project [12], a project whose purpose was to compare and validate upscaling techniques. The heterogeneity model is sampled from a Brent sequence from the North Sea and contains two formations: a shallow-marine Tarbert formation and a fluvial Upper Ness formation.

The paper is organised as follows. In Section 2 we present the differential equations that govern immiscible and incompressible two-phase flow. The concept behind streamline methods is outlined in Section 3 and MMsFEM is described in Section 4. Section 5 discusses construction of efficient solvers for linear systems that arise from the mixed formulation of the pressure equation. Numerical results are presented in Section 6, and we conclude with some final remarks in Section 7.

2 Mathematical model of two-phase flow

The differential equations modelling immiscible and incompressible two-phase flow can be derived from the continuity equation of each phase

$$\phi\frac{\partial S_i}{\partial t} + \nabla \cdot v_i = q_i \tag{1}$$

and Darcy's law that relates the phase velocities v_i to the gradient of the phase pressures p_i

$$v_i = -K\lambda_i(\nabla p_i - \rho_i G). \tag{2}$$

Here ϕ denotes porosity; S_i is the saturation of phase i; q_i is a source term representing wells; K is the rock permeability tensor, assumed to be symmetric and uniformly positive definite; and $\lambda_i = k_{ri}/\mu_i$ is the mobility of phase i. The relative permeability k_{ri} models the reduced permeability experienced by one phase due to the presence of the other, and μ_i is the phase viscosity. Finally, ρ_i is the phase density, and G is the gravity acceleration vector. We shall assume

4

that the phases are oil (o) and water (w) and that the two phases together fill the void space completely so that $S_o + S_w = 1$. The phase pressures are related in terms of the capillary pressure $p_{cow} = p_o - p_w$, which we assume, according to common practice, is a known function of water saturation, $p_{cow}(S_w)$.

In this paper we will work with the fractional flow formulation of the two-phase flow model consisting of an equation for a global pressure and a transport equation for the water saturation. By summing the Darcy equations (2) for oil and water, we derive

$$v = -K\lambda_t(\nabla p_o - f_w \nabla p_{cow}) + K(\lambda_o \rho_o + \lambda_w \rho_w)G.$$

Here f_w is the fractional flow function of water given by $f_w = \lambda_w/\lambda_t$, where $\lambda_t = \lambda_w + \lambda_o$ denotes the total fluid mobility. Assume now that there exists an auxiliary function $p_c = p_c(S_w)$ such that $\nabla p_c = f_w \nabla p_{cow}$ and define the global pressure $p = p_o - p_c$. By summing the continuity equations (1) and using that $S_w + S_o = 1$, we derive equations for the global pressure p and the total velocity $v = v_w + v_o$,

$$v = -K\Big[\lambda_t \nabla p - (\lambda_o \rho_o + \lambda_w \rho_w)G\Big], \qquad \nabla \cdot v = q. \tag{3}$$

Finally, we use (1) to derive a mass-transport equation for the water phase. To this end, we need an expression for the water velocity. By a straightforward manipulation of $\lambda_o v_w - \lambda_w v_o$ using (2) we obtain

$$v_w = f_w\Big[v + K\lambda_o(\rho_w - \rho_o)G + K\lambda_o \frac{\partial p_{cow}}{\partial S_w}\nabla S_w\Big].$$

The main focus of the paper is to show that multiscale methods can be combined with streamline-based simulation to give rapid reservoir performance predictions. We therefore neglect effects from capillary forces so that the final form of the saturation equation becomes

$$\phi \frac{\partial S_w}{\partial t} + \nabla \cdot f_w\Big[v + K\lambda_o(\rho_w - \rho_o)G\Big] = q_w. \tag{4}$$

In streamline simulation a simple sequential splitting is used to decouple and solve the coupled system (3)–(4) (sometimes called IMPES or sequential splitting). First, the initial saturation distribution is used to compute the mobilities in (3) and the equation is solved for global pressure and total velocity. Then, the total velocity is held constant as a parameter in (4), while the saturation is advanced in time. This completes one step of the method. Next, the new saturation values are used to update the mobilities in (3), the pressure equation is solved again, and so on. Numerical methods for solving (3) and (4) will be presented in the next two sections. For brevity we hereafter drop the subscript w and let S denote water saturation.

3 A streamline method for two-phase flow simulation

The saturation equation (4) is solved using a streamline method. For simplicity, we assume incompressible flow and neglect gravity and source terms. Then the saturation equation (4) reads

$$\phi \partial_t S + v \cdot \nabla f(S) = 0.$$

Streamlines are flow-paths traced out by a neutral particle being passively advected by a flow field so that the velocity v is tangential to the streamline at every point. For incompressible flow, for which the velocity field v is divergence-free and irrotational, all streamlines start in an injector and end in a producer. Moreover, individual streamlines do not cross and there is no mass transfer between individual streamlines. Each streamline can therefore be viewed as an isolated flow system and we may transform (4) into a family of one-dimensional equations along streamlines. To this end, we introduce the so-called *time-of-flight* coordinate $\tau = \tau(x)$, which measures the time it takes a passive particle released in one of the injectors at time zero to travel along the streamlines with speed $|v|/\phi$ and reach a point x in physical space. Thus, along any streamline the associated time-of-flight coordinate must satisfy the differential equation

$$v \cdot \nabla \tau = \phi \qquad \text{or equivalently} \qquad \partial \tau = \phi/|v| \, ds. \tag{5}$$

Integrating the latter equation along a streamline Ψ from $x_0 = \Psi(s_0)$ to $x = \Psi(s)$ gives

$$\tau(s) - \tau(s_0) = \int_{s_0}^{s} \frac{(\phi \circ \Psi)(\xi)}{|(v \circ \Psi)(\xi)|} \, d\xi. \tag{6}$$

By invoking the operator identity $\partial/\partial \tau = v \cdot \nabla$, the multidimensional saturation equation now reduces to a family of one-dimensional equations along each streamline Ψ,

$$\partial_t S + \partial_\tau f_w = 0. \tag{7}$$

In streamline methods one often neglects the effects of gravity (as we will do in this paper). If gravity is important, it can be incorporated through operator splitting [13]; that is, by first solving (7) along all streamlines, and then solving

$$\phi \partial_t S + \nabla \cdot \left[f_w K \lambda_o (\rho_w - \rho_o) G \right] = 0 \tag{8}$$

along gravity lines initiated in the top layer of cells in the reservoir. This operator splitting is also the industry standard and is implemented in the commercial streamline simulators FrontSim and 3DSL.

To trace the flow paths we use an algorithm introduced by Pollock [14] for regular quadrilateral or hexahedral grids. (See [15] for an extension to irregular grids). The method builds each streamline in a cell-by-cell manner: Given the entry point and a piecewise linear velocity in each direction, Pollock's algorithm computes analytically the exit point and the grid-block time-of-flight $\Delta\tau_i$, i.e., the time it takes for the streamline to traverse the grid block. Within each cell, the saturation value is constant, and by picking up these values, one obtains a piecewise initial value function for (7) given on an irregular grid $\{\Delta\tau_i\}$ for each streamline. This initial-value problem can then be solved by one's favourite one-dimensional solver; here we will use a front-tracking method. After the initial saturation profile has been advected along the streamlines, the updated saturation values are projected back onto the original grid by weighting the contributions from the individual streamlines according to the associated traversal time $\Delta\tau_i$ through the grid cell.

Note that the streamline method does not require that one represents the streamline geometry explicitly. Indeed, all one needs is the time-of-flight value through each cell and the corresponding saturation value. Since this cell-by-cell parametrisation often results in a highly irregular grid in τ with small cells close to the boundaries (where the wells are located), simulators that use finite-volume methods along each streamline tend to use a uniform and possibly coarsened grid to speed up the computation.

To solve the one-dimensional transport equations (7) and (8) along streamlines and gravity lines we will use a front-tracking method, which is sometimes called wave-front-tracking or Dafermos' method. See Holden and Risebro [16] for a complete list of references and a thorough introduction to the method. In the front-tracking method the solution of the tranport equation is represented as a set of moving discontinuities. The solution is evolved in time by tracking the discontinuities along space-time rays and resolving a Riemann problem each time two or more rays collide. To ensure that the solution is always piecewise constant, the self-similar Riemann problems are approximated by step functions in which shocks are kept and rarefactions are discretised by a series of small steps.

The reason for using this particular method is that it is independent of a grid, very fast, unconditionally stable, and has first order convergence with respect to the approximation of the Riemann solutions (and the initial data). In particular, this means that the method is perfect for handling the highly irregular grids arising from the streamline parametrisations. Moreover, the method resolves water fronts sharply with *no* numerical diffusion. Hence, the numerical diffusion inherent in the corresponding streamline method for two-phase flow comes from the projection of the saturation profiles along the streamlines (and gravity lines) onto the original grid, see e.g., [13].

4 A mixed multiscale FEM

We now introduce a mixed FEM that will be used to solve the elliptic pressure equation (3). The method, which was introduced in [1], is a modified version of the mixed multiscale FEM (MMsFEM) proposed by Chen and Hou [9]. Our method differs from the one of Chen and Hou in two important ways. First, it gives a mass conservative velocity field at the subgrid scale. This means that the MMsFEM solution for the velocity variable can be used to simulate phase transport at the subgrid scale. Second, as it is very important to have proper boundary conditions for the base functions to achieve high accuracy, we propose to use boundary conditions that reflect local heterogeneous structures and account for a radial flow-pattern in near-well regions.

Another issue that will be treated here, that was not addressed in [1], is how to treat the wells within the multiscale framework if the well-rates are not known a priori. This is an issue of high practical importance since the production well-rates are seldom known a priori, but are instead specified by the bottom-hole pressure in each well. We therefore propose a new well-model for the MMsFEM that naturally exploits available subgrid information. It is well known that to obtain an accurate flow scenario it is important to capture the fine-scale flow behaviour in the vicinity of the wells. We therefore believe that the modified MMsFEM with the proposed well-model, provides a step towards more robust and rigorous treatment of wells in reservoir simulation. We start by introducing the mixed formulation of (3) with no-flow boundary conditions.

Let Ω denote the reservoir domain and n be the outward pointing unit normal on $\partial\Omega$. Moreover, define the function space

$$H_0^{1,\mathrm{div}}(\Omega) = \{v \in (L^2(\Omega))^d : \ \nabla \cdot v \in L^2(\Omega) \text{ and } v \cdot n = 0 \text{ on } \partial\Omega\}.$$

Then the mixed formulation of (3) with no-flow boundary conditions $v \cdot n = 0$ on $\partial\Omega$ reads: find $(p, v) \in L^2(\Omega) \times H_0^{1,\mathrm{div}}(\Omega)$ such that

$$\int_\Omega (K\lambda_t)^{-1} v \cdot u \, dx - \int_\Omega p \, \nabla \cdot u \, dx = \int_\Omega (f_w \rho_w + f_o \rho_o) G \cdot u \, dx,$$
$$\int_\Omega l \, \nabla \cdot v \, dx = \int_\Omega ql \, dx, \tag{9}$$

for all $u \in H_0^{1,\mathrm{div}}(\Omega)$ and $l \in L^2(\Omega)$.

Equation (9) is discretised by dividing Ω into polyhedral (coarse grid) elements $\mathcal{T} = \{T\}$. In mixed FEMs, the approximation space for the velocity v is spanned by a set of base functions $\{\psi\}$ in $H_0^{1,\mathrm{div}}(\Omega)$. In the proposed MMsFEM, each base function is associated with an interface $\Gamma_{ij} = \partial T_i \cap \partial T_j$ between two coarse grid blocks T_i and T_j. To be specific, for each interface Γ_{ij} we define an interface flux $\psi_{ij} = -K\lambda_t \nabla \phi_{ij}$, where ϕ_{ij} is determined by solving the following "pressure equations" numerically on a fine-scale subgrid within the coarse blocks T_i and T_j

$$(\nabla \cdot \psi_{ij})|_{T_i} = \begin{cases} 1/|T_i|, & \text{if } \int_{T_i} q \, dx = 0, \\ q/\int_{T_i} q \, dx, & \text{otherwise}, \end{cases} \tag{10}$$

$$(\nabla \cdot \psi_{ij})|_{T_j} = \begin{cases} -1/|T_j|, & \text{if } \int_{T_j} q \, dx = 0, \\ -q/\int_{T_j} q \, dx, & \text{otherwise} \end{cases} \tag{11}$$

with some compatible boundary conditions

$$\psi_{ij} \cdot n = 0 \text{ on } \partial T_i \cup \partial T_j \backslash \Gamma_{ij} \qquad \text{and} \qquad \psi_{ij} \cdot n_{ij} = \nu_{ij} \text{ on } \Gamma_{ij}. \tag{12}$$

Here n is the outward unit normal on $\partial(T_i \cup \Gamma_{ij} \cup T_j)$ and n_{ij} is the unit normal to Γ_{ij} pointing from T_i to T_j. The corresponding approximation space for the total Darcy velocity v is now spanned by the base functions $V^{ms} = \mathrm{span}\{\psi_{ij} : \mathrm{meas}(\Gamma_{ij}) > 0\}$. The boundary condition ν_{ij} that we impose on Γ_{ij} in (12) will be specified in Section 4.3.

The local pressure solutions ϕ_{ij} do not appear explicitly in the mixed formulation, and are hence only used to generate the base functions ψ_{ij}. Since it is important that all base functions are mass conserving, the subgrid problems (10)–(11) must be solved using a mass conservative method, e.g., a suitable mixed FEM or a finite-volume method. The particular choice of method depends in part on the local grid structure. For instance, if we want to discretise the subgrid problems with a finite-volume method, then a two-point flux approximation can be used if K is a diagonal tensor and the grid is orthogonal, whereas a multi-point flux approximation scheme should be used on non-orthogonal grids.

Also note that the base functions ψ_{ij} will generally be time dependent since they depend on λ_t, which is time dependent through $S_w(x,t)$. This indicates that one has to regenerate the base functions for each time step. However, it is usually sufficient to regenerate a small portion of the base functions at each time step since the total mobility λ_t only varies significantly in the vicinity of the propagating saturation front; similar observations have been made for the multiscale finite-volume method developed by Jenny et al. [10]. In [1], Aarnes

suggested that one should regenerate a base function ψ_{ij} only if

$$\int_{T_i} \lambda_t \, dx \quad \text{or} \quad \int_{T_j} \lambda_t \, dx \tag{13}$$

have changed more than some threshold since the previous update. This criteria is a bit crude, but performs well, as is demonstrated in [1], as long as one is able to specify a sensible threshold value.

4.2 The approximation space for the pressure

In the original version of the MMsFEM, Chen and Hou used a piecewise constant approximation for the pressure, $p \in U := \mathcal{P}_0(\mathcal{T})$. This was a natural choice since the approximation spaces for the Darcy velocity v and pressure p satisfied $U = \text{div}(V^{ms})$, a relation that guarantees that the method is stable. However, by altering the base functions to produce mass conservative velocity fields, this relation no longer holds true, and Aarnes [1] argued that one also needs to modify the approximation space for the pressure p. The argument goes as follows.

Assume that (p, v) solves the (not discretised) mixed formulation (9) on the fine-scale grid and let the boundary conditions for the MMsFEM base functions be defined by $\nu_{ij} = v|_{\Gamma_{ij}}$ so that $v \in V^{ms}$. Furthermore, write $p = \bar{p} + \hat{p}$, where $\bar{p} \in U$ is a constant on the coarse grid and $\hat{p}$ is the subgrid variation in pressure that has zero average over all coarse grid blocks $T \in \mathcal{T}$. If we now assume that $\hat{p}$ is known a priori and move it over to the right hand side, then, since $V^{ms} \subset H_0^{1,\text{div}}(\Omega)$ and $U \subset L^2(\Omega)$, we find that $(\bar{p}, v) \in U \times V^{ms}$ satisfies

$$\int_{\Omega} (K\lambda_t)^{-1} v \cdot u \, dx - \int_{\Omega} \bar{p} \, \nabla \cdot u \, dx = \int_{\Omega} \hat{p} \, \nabla \cdot u \, dx + \int_{\Omega} (f_w \rho_w + f_o \rho_o) G \cdot u \, dx,$$
$$\int_{\Omega} l \, \nabla \cdot v \, dx = \int_{\Omega} q l \, dx,$$

$$\tag{14}$$

for all $u \in V^{ms}$ and $l \in U$. This shows that in the presence of exact boundary conditions ν_{ij} for the base functions, and under the assumption that $\hat{p}$ is known a priori, we can find the solution (p, v) of the mixed formulation (9) by solving the modified equation (14) for $(\bar{p}, v)$ in the finite-dimensional space $U \times V^{ms}$ and setting $p = \bar{p} + \hat{p}$.

Assuming $p = \bar{p} \in U$ means that the sub-scale variation in pressure is disregarded. In other words, we neglect the integral $\int \hat{p} \nabla \cdot u dx$ and thus make an error in the computation of $\bar{p}$. Numerical experience shows that the block-average pressures $\bar{p}$ are quite sensitive to $\hat{p}$ so that $\bar{p}$ will be inaccurate if we neglect the (significant) contribution from $\hat{p}$. This observation suggests that

it *is* necessary to modify the approximation space for pressure in the formulation of MMsFEM, and that an appropriate approximation space should be close to the affine space $\hat{U} = \hat{p} + U$. Unfortunately, $\hat{p}$ is never known a priori. If it were, then we would not have to solve the pressure equation at all since for incompressible flows one is only interested in the velocity field. However, $\int_T \hat{p} \, \nabla \cdot u \, dx$ vanishes everywhere except where $\int_T q \, dx \neq 0$. Thus, $\hat{p}$ only contributes to $\int_T p \, \nabla \cdot u \, dx$ in the well-blocks. This indicates that if we can find a function $\tilde{p}$ that approximates $\hat{p}$ in the well blocks and vanishes elsewhere, we should get good accuracy by replacing $\hat{p}$ in (14) with $\tilde{p}$.

To compute $\tilde{p}$, let T be a well-block and define $\tilde{p}$ in T according to

$$
\int_T \tilde{p} = 0, \qquad \tilde{v} = -K \left[\lambda_t \nabla \tilde{p} - (\lambda_o \rho_o + \lambda_w \rho_w) G \right],
$$
$$
\nabla \cdot \tilde{v} = q \text{ in } T, \qquad \tilde{v} \cdot n = \nu_T \text{ on } \partial T. \tag{15}
$$

The boundary condition ν_T will, along with the boundary conditions for the base functions, be specified in Section 4.3. The modified MMsFEM in [1] now seeks $p \in \tilde{p} + U$ and $v \in V^{ms}$ such that (9) holds for all $l \in U$ and $u \in V^{ms}$. Henceforth we will, for brevity, refer to this method simply as MMsFEM.

4.3   Selection of boundary conditions

The boundary condition ν_{ij} that we impose on Γ_{ij} in the definition of the base functions (10)–(12) plays a special and very important role in the MMsFEM. Indeed, since we seek the Darcy velocity v in V^{ms} it is clear that $v|_{\Gamma_{ij}} \in \text{span} \, \nu_{ij}$. The local flow behaviour across each interface is therefore completely determined, up to a constant multiple, by the selection of the boundary conditions for the base functions. It is therefore essential that these boundary conditions reflect some of the dominating features that have an impact on the local flow behaviour, including heterogeneous structures that penetrate the interfaces and radial flow patterns in the proximity of wells. The same can be said about the boundary conditions ν_T that we use to compute $\tilde{p}$.

In this section we describe two alternative strategies that can be used to prescribe boundary conditions for $\tilde{p}$ and the base functions. The first approach is a local approach where we assume no a priori knowledge about the actual flow pattern. In the second approach, which is more robust but also computationally more expensive, we assume that the pressure equation (3) can be solved once on a fine grid. This is a reasonable assumption. Indeed, since multigrid preconditioning techniques give linear complexity, and all base functions must be computed at least once, the cost of solving the pressure equation (3) on the subgrid is comparable to cost of the initial construction of the base functions.

4.3.1   Local boundary conditions

We want the local boundary conditions to reflect heterogeneous structures that penetrate the interfaces and account for a radial flow pattern in the near-well regions. In addition, we need to ensure compatibility. These requirements are fulfilled in the following definition

$$\nu_T(x) = \frac{q_T \nu_T^0(x)}{\int_{\partial T} \nu_T^0(s) \, ds}, \quad x \in \partial T, \tag{16}$$

$$\nu_{ij}(x) = \frac{\nu_{ij}^0(x)}{\int_{\Gamma_{ij}} \nu_{ij}^0(s) \, ds}, \quad x \in \Gamma_{ij}, \tag{17}$$

where $q_T = \int_T q(\xi) \, d\xi$ and

$$\nu_T^0 = n_T \cdot (wK\lambda_t) \cdot n_T, \tag{18}$$

$$\nu_{ij}^0 = n_{ij} \cdot (wK\lambda_t) \cdot n_{ij}. \tag{19}$$

Here the purpose of w is to account for a radial flow pattern near wells. Hence, on the boundary of a well-block, we define w according to

$$w(x) = \int_T \frac{|q(\xi)|}{|x - \xi|^{1-d}} \, d\xi.$$

If Γ_{ij} is not a well block interface, then we do not want a contribution from w, and we set $w \equiv 1$ in (19). The exponent $1 - d$ is motivated by the observation that if we have uniform radial flow around a point source at $z \in T$, then the flow velocity across ∂T must scale proportional to $\mathrm{dist}(x, z)^{1-d}$ to preserve mass.

Figures 1 and 2 display corresponding base functions for a two-dimensional model with homogeneous and random coefficients, respectively. The base functions depicted in the top rows of each figure correspond to an interface away from the near-well region and the base functions depicted in the bottom rows correspond to a well-block interface. We see that the top row base function in Figure 1 is identical to the associated base function for the Raviart–Thomas mixed FEM of lowest order. In contrast, we observe that the base function corresponding to random coefficients fluctuates rapidly and clearly reflects the fine-scale details in the heterogeneous formation. We also note that the interface is hardly visible in the base function depicted in the bottom row of Figure 1. This demonstrates that the radial-distance weighting used in the near-well region accounts for the radial flow pattern in a proper way. The location of the well itself is reflected in the delta-like peaks seen in the x-component of the base functions.
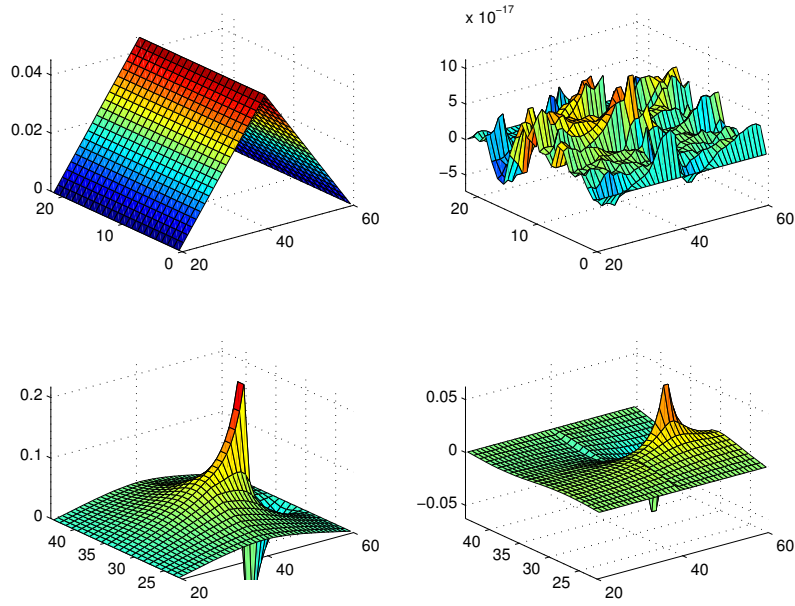
Fig. 1. The x-component (left) and y-component (right) of two MMsFEM base functions for a two-dimensional model with homogeneous coefficients using the local boundary conditions defined by (17) and (19). The top base function corresponds to an interface away from the near-well region while the bottom base function corresponds to a well-block interface.
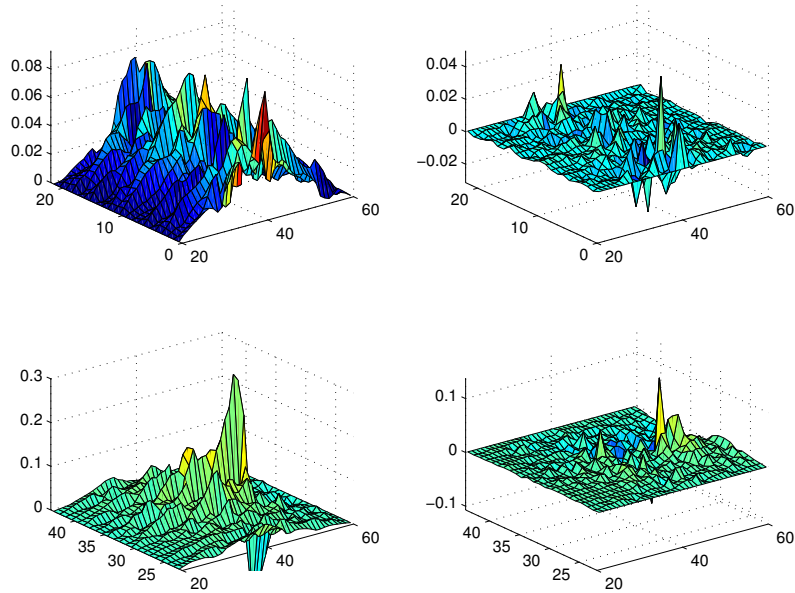

Fig. 2. The x-component (left) and y-component (right) of two MMsFEM base functions for a two-dimensional model with random coefficients using the boundary conditions defined by (17) and (19). The top base function corresponds to an interface away from the near-well region while the bottom base function corresponds to a well-block interface.

13

4.3.2 Global boundary conditions

We now assume that the initial velocity field v^0 is available on the fine grid. The so-called global boundary conditions are now determined by defining ν_{ij}^0 and ν_T^0 in (16)–(17) for $t > t_0$ according to

$$\nu_T^0(x,t) = \frac{\lambda_t(x,t)}{\lambda_t(x,t_0)}(v^0 \cdot n_T), \quad x \in \partial T, \ t > t_0. \tag{20}$$

$$\nu_{ij}^0(x,t) = \frac{\lambda_t(x,t)}{\lambda_t(x,t_0)}(v^0 \cdot n_{ij}), \quad x \in \Gamma_{ij}, \ t > t_0, \tag{21}$$

These boundary conditions reflect, not only features that have a local impact on the flow, but also global effects from, e.g., fractures, faults, well configurations, and external boundary conditions.

Remark 1 *In (16) we assumed that the well-rates are specified. If the well-rates instead are determined by the bottom-hole pressure, the well-rates q_T in (16) on the coarse grid are approximated from the well-rates induced by the MMsFEM solution on the coarse grid in the previous time step. To be precise, if q_w are the previous subgrid well-rates for a well w, then well-rates at the next time step t_{m+1} are defined by*

$$q_w(x, t_{m+1}) = (q_w^0/Q_w^0)q_T, \tag{22}$$

where $q_w^0 = q_w(x, t_m)\lambda_t(x, t_{m+1})/\lambda_t(x, t_m)$, q_T is the total grid-block well-rate from the previous time step, and Q_w^0 is the total of the subgrid well-rates q_w^0. The coarse grid well rates that appear in (16) at time t_{m+1} are now defined as the sum of the subgrid well-rates $q_w(x, t_{m+1})$. If local boundary conditions are used, the initial well-rates can be determined from e.g., an auxiliary upscaled model.

4.4 Well-model

In a Peaceman-type well-model the well-rate in a cell i is linearly related to the difference between the cell pressure p_i and the bottom-hole pressure p_{bhp}

$$q_i = -T_{w,i}(p_i - p_{\text{bhp}}). \tag{23}$$

The so-called *well transmissibility* $T_{w,i}$ is defined by some semi-analytical relation [17]. Since, for pressure constrained wells, the well-block source terms in (10)–(11) are not known a priori, the subgrid well-rates are determined by a rate constrained Peaceman model. That is, we assume that the total well-rate for each well-block is equal to one. Similarly, when solving (15) we use a rate-constrained well-model and assume that the total well-rate Q_w is equal to the associated well-rate q_T^0 from the previous time step.

To define a corresponding well-model for the MMsFEM, we need to define a similar relation between the total well-rate q_T in a coarse grid block and the average pressure $\bar{p}_T$ in the well-block. To this end, recall first that $p_T = \bar{p}_T + \tilde{p}_T$ approximates the subgrid pressure in T. This relation suggests that we can define a multiscale well-model based on the accumulated well-rates induced by p_T and the (Peaceman type) well-model that is used to compute $\tilde{p}_T$

$$q_T = - \sum_{i \in T} T_{w,i} (\bar{p}_T + \tilde{p}_{T,i} - p_{\text{bhp}}). \tag{24}$$

Here the well transmissibility $T_{w,T} = \sum_{i \in T} T_{w,i}$ on the coarse grid will enter in the linear system as a diagonal component in the lower right hand block of the MMsFEM coefficient matrix and $\tilde{q} = - \sum_{i \in T} T_{w,i} (\tilde{p}_{T,i} - p_{\text{bhp}})$ will enter into the right hand side.

It is important to note that the well-rates q_T on the coarse grid induced by (24) will in general not coincide with the corresponding well-rates that appear in (16), which are defined by (22). Indeed, in (22) it is implicitly assumed that the total grid-block well-rates at time t_{m+1} are equal to the corresponding MMsFEM induced well-rates at time t_m. The MMsFEM well-model (24), on the other hand, allows the grid-block well-rates to vary in time.

4.5   Computational considerations

As noted in the introduction, the possibility of accelerated simulations is one of the main motivation factors for using a multiscale method for reservoir simulation. In the simulation results that we will present here, the MMsFEM base functions have been regenerated for each time step. This implies that the method will, with efficient implementation, have linear complexity. Hence the computational cost will be comparable to the cost of solving the full fine-scale pressure equation using an efficient multigrid technique. This is also in accordance with our observations. For the MMsFEM, however, several steps can be taken that can accelerate the computation time considerably.

First, as we have already pointed out, the MMsFEM base functions should be updated only in regions where the total mobility has changed significantly since the previous update. Aarnes [1] observed that the accuracy obtained when updating a small fraction of the base functions (mostly near saturation fronts) in each time step is almost the same as when updating all base functions (see also [10]). Since the calculation of the base functions dominates the computation time in the MMsFEM, adaptive calculation of the base functions can accelerate solution procedure for the pressure equation one order of magnitude.

Another way of accelerating MMsFEM based simulations is by parallel computing. Computation of base functions can be done on a block-by-block basis and has an obvious parallelism. Similarly, the numerical integration over base functions used to assemble the linear system that arises from the mixed formulation (9) on the coarse grid is also inherently parallel. These computations can therefore be assigned to individual processors, and are well suited for both distributed memory and shared memory platforms. However, to fully take advantage of parallel computing, we should also parallelise the solution procedure for mixed linear system. Since such systems are indefinite, standard parallelisable domain decomposition techniques and multigrid techniques cannot be used directly. Instead, parallel preconditioners must be applied inside an iterative procedure such as preconditioned GMRES algorithm (see, e.g., [18]) or a preconditioned (inexact) Uzawa algorithm (see, e.g., [19]). Below we describe in detail two possible strategies for solving the indefinite linear system that can take advantage of parallel preconditioners for positive definite systems (e.g., multigrid and domain decomposition techniques).

5   Numerical linear algebra

The MMsFEM methodology offers subgrid resolution, and should give high accuracy with upscaling factors of more than one order of magnitude in each coordinate direction. Nevertheless, since geological reservoir characterisations today may involve grids with 10^7–10^9 grid blocks, MMsFEM does not remove the need for efficient numerical linear algebra. We therefore present a strategy that can be used to design efficient iterative methods for linear systems that arise from the MMsFEM formulation of (3). For presentational simplicity we assume that all well-rates are specified, i.e., that no well-model is used.

5.1   Preconditioning

The linear system arising from the MMsFEM formulation of (3) is

$$
\begin{bmatrix} \mathbf{B} & \mathbf{C^T} \\ \mathbf{C} & \mathbf{0} \end{bmatrix} \begin{bmatrix} \mathbf{v} \\ \mathbf{p} \end{bmatrix} = \begin{bmatrix} \mathbf{g} \\ -\mathbf{q} \end{bmatrix},
\tag{25}
$$

where

$$\mathbf{B} = [\int_\Omega (K\lambda_t)^{-1}\psi_{ij} \cdot \psi_{kl} \, dx], \qquad\qquad \mathbf{C} = [-\int_{T_m} \mathrm{div}(\psi_{ij}) \, dx],$$

$$\mathbf{g} = [\int_\Omega \tilde{p} \, \mathrm{div}(\psi_{kl}) + (f_w\rho_w + f_o\rho_o)G \cdot \psi_{ij} \, dx,], \qquad \mathbf{q} = [\int_{T_m} q \, dx].$$

Since pure Neumann boundary conditions are imposed on $\partial\Omega$, the linear systems (25) is singular, but it is made non-singular by specifying the pressure level, e.g., by specifying the pressure in one grid block T. If $\mathbf{v} = [v_{ij}]_{\Gamma_{ij} \neq \emptyset}$ and $\mathbf{p} = [p_m]_{T_m \in \mathcal{T}}$ solves (25), then $v = \sum_{ij} \mathbf{v}_{ij} \psi_{ij}$ and $p = \tilde{p} + \sum_m \mathbf{p}_m \chi_{T_m}$ is the desired MMsFEM solution.

Now, since (25) stems from (9), it is an indefinite linear system and this limits the number of suitable iterative methods. However, we may exploit the block structure in the MMsFEM coefficient matrix to reduce (25) to three symmetric and positive definite systems

$$\mathbf{Bu} = \mathbf{g}, \tag{26}$$
$$\mathbf{Sp} = \mathbf{q} + \mathbf{Cu}, \tag{27}$$
$$\mathbf{Bv} = \mathbf{g} - \mathbf{C^T p}. \tag{28}$$

where $\mathbf{S} = \mathbf{CB^{-1}C^T}$. Clearly, we can in general not afford to compute $\mathbf{S}$ directly since this requires that we compute the $\mathbf{B^{-1}}$ explicitly. Fortunately, one of the most powerful iterative methods methods for positive definite linear systems, the preconditioned conjugate gradient (PCG) method, only requires that we compute the action of $\mathbf{S}$.

A simple and efficient preconditioner for $\mathbf{S}$ is the sparse matrix $\mathbf{M} = \mathbf{CD^{-1}C^T}$, where $\mathbf{D}$ is the diagonal part of $\mathbf{B}$. In fact, $\mathbf{M}$ is the matrix that arises from a standard finite-volume scheme using a two-point flux approximation if the transmissibility for Γ_{ij} is the associated component of $\mathbf{D^{-1}}$, $d_{ij,ij} = (\int_\Omega (K\lambda_t)^{-1} \psi_{ij} \cdot \psi_{ij} \, dx)^{-1}$. The PCG algorithm for (27) with $\mathbf{M}$ as the preconditioner should now converge in a small number of iterations. Algorithm 5.1 now outlines how one should compute the solution of the linear system (27).

Algorithm 1 The preconditioned conjugate gradient method

Solve $\mathbf{Bu} = \mathbf{g}$ and compute $\mathbf{w} = \mathbf{q} + \mathbf{Cu}$.
Pick an initial guess $\mathbf{p_0}$ for $\mathbf{p}$.
Set $\mathbf{r_0} = \mathbf{w} - \mathbf{Sp_0}$, $\mathbf{z_0} = \mathbf{M^{-1}r_0}$ and $\mathbf{s_0} = \mathbf{z_0}$.
For $j = 0, 1, \ldots,$ *until convergence*, do
$\quad \mathbf{y_j} = \mathbf{Sp_j}$
$\quad \alpha = (\mathbf{r_j}, \mathbf{z_j})/(\mathbf{s_j}, \mathbf{y_j})$
$\quad \mathbf{p_{j+1}} = \mathbf{p_j} + \alpha \mathbf{s_j}$
$\quad \mathbf{r_{j+1}} = \mathbf{r_j} - \alpha \mathbf{y_j}$
$\quad \mathbf{z_{j+1}} = \mathbf{M^{-1}r_{j+1}}$
$\quad \beta = (\mathbf{r_{j+1}}, \mathbf{z_{j+1}})/(\mathbf{r_j}, \mathbf{z_j})$
$\quad \mathbf{s_{j+1}} = \mathbf{z_{j+1}} + \beta \mathbf{s_j}$.

Note that each iteration of Algorithm 4.1 involves the action of $\mathbf{S}$, and hence of $\mathbf{B^{-1}}$, as well as the action of $\mathbf{M^{-1}}$. This implies that we need to solve two sparse, symmetric and positive definite systems in each iteration. These

systems can be solved efficiently with the PCG method using a multigrid or domain decomposition preconditioner. When we solve the systems with matrix $\mathbf{B}$, we need to choose the same, or a stronger, convergence criteria as the convergence criteria for the outer iteration. If we do not, the accuracy will deteriorate. On the other hand, since $\mathbf{M}$ is only a preconditioner, we do not have to have the same convergence criteria for the systems with matrix $\mathbf{M}$, but a weak convergence criteria will cause the number of outer iterations to increase.

5.2 Compressible Flow

At this point it is appropriate to make some comments related to the preconditioning of linear systems that arise from the mixed formulation of the pressure equation in compressible flow problems. This is because the (slightly) parabolic nature of the compressible two-phase flow pressure equation introduces a diagonal matrix in the lower right hand block of the MMsFEM coefficient matrix. Indeed, for compressible flow problems one replaces (3) with a pressure equation that is qualitatively on the form

$$
v = -K\Big[\lambda_t \nabla p - (\lambda_o \rho_o + \lambda_w \rho_w)G\Big], \qquad \nabla \cdot v + c\frac{\partial p}{\partial t} = q, \tag{29}
$$

where $c = c(x,t)$ is a positive scalar function. This implies that the second equation in (9) transforms to

$$
\int_\Omega l\,\nabla \cdot v\,dx + \int_\Omega lc\frac{\partial p}{\partial t} = \int_\Omega ql\,dx. \tag{30}
$$

In the MMsFEM discretisation, the second integral on the left hand side will now give rise to a positive diagonal matrix $\mathbf{U}$ so that the corresponding coefficient matrix for compressible flow problems becomes:

$$
\begin{bmatrix} \mathbf{B} & \mathbf{C^T} \\ \mathbf{C} & -\mathbf{U} \end{bmatrix}. \tag{31}
$$

Since $\mathbf{U}$ is non-singular, the Schur complement matrix with respect to $\mathbf{U}$ is

$$
\mathbf{S} = \mathbf{B} + \mathbf{C^T U^{-1} C}. \tag{32}
$$

This Schur complement matrix can be computed explicitly at a low cost and is, unlike the Schur complement matrix with respect to $\mathbf{B}$, sparse and has the same sparsity structure as $\mathbf{B}$. Moreover, if the time step is small, then the condition number of $\mathbf{S}$ is close to that of $\mathbf{B}$ and the PCG method with an effective preconditioner — for instance a sweep of a multigrid or domain decomposition algorithm — should converge quickly, and does not involve the solution

of additional linear systems in the iterative loop. Hence, for compressible flow problems, the preconditioning of the linear system that arises from the mixed formulation (9) is less of a challenge. However, if the time step is very large, or if compressibility effects are negligible, the ill-conditioning of the divergence matrix $\mathbf{C^T C}$ can influence the condition number of $\mathbf{S}$ and we might want to use the alternative Schur decomposition in (27).

6 Numerical examples

In this section we will demonstrate that the MMsFEM-streamline is a robust and viable alternative to upscaling-based reservoir simulation schemes. We apply the current methodology to two test-cases with data taken from the second model in the tenth SPE comparative solution project (SPE 10) [12]. The model was designed to benchmark different upscaling techniques and is therefore a good test case for our methodology.

The reservoir model consists of a Tarbert formation in the top 35 layers and an Upper Ness sequence in the bottom 50 layers, see Figure 3. The permeability tensor is a diagonal tensor with equal permeability in the two horizontal coordinate directions: $K_x = K_y$. Both formations are characterised by large permeability variations, 8–12 orders of magnitude, but are qualitatively different, as can be seen from Figure 4. While the Tarbert formation has relatively smooth permeability variations, the Upper Ness formation is fluvial and contains channels that make the formation particularly hard to upscale. The porosity field is strongly correlated to the permeability, and about 2.5% of the blocks have zero porosity and are therefore considered to be inactive.

The physical parameters are as given in [12], except that we neglect compressibility and gravity for simplicity in our simulations. The relative permeability curves are given as

$$k_{rw} = (S^*)^2, \qquad k_{ro} = (1 - S^*)^2, \qquad S^* = \frac{S - S_{\text{wc}}}{1 - S_{\text{wc}} - S_{or}}, \tag{33}$$

with $S_{\text{wc}} = S_{\text{or}} = 0.2$. The initial saturation is $S_0 \equiv S_{\text{wc}}$. Oil and water viscosities are $\mu_o = 3.0$ cP and $\mu_w = 0.3$ cP, respectively, and the water injection rate is 5000 bbl. per day. Each of the four producers are specified to produce at 4000 psi bottom-hole pressure.

We compare solutions obtained with MMsFEM, using both the local boundary conditions determined by (16)–(19) and the global conditions determined by (16)–(17) and (20)–(21). To validate the performance of MMsFEM, these solutions are compared with a reference solution obtained by solving the pressure equation (3) directly at the subgrid scale using a finite-volume scheme
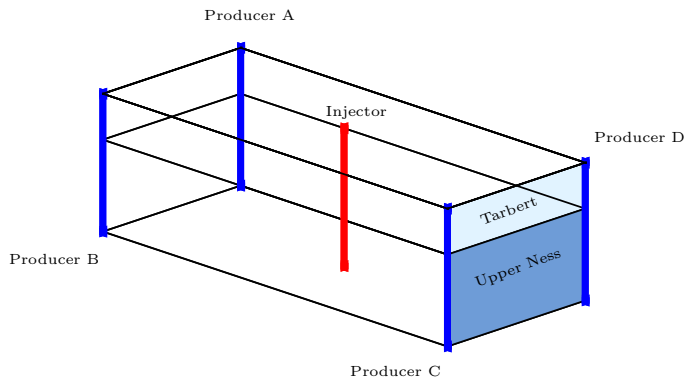
19

Fig. 3. Well configuration for reservoir model used in the tenth SPE comparative solution project. The model dimensions are $1200 \times 2200 \times 170$ ft, and the fine and coarse meshes consist of $60 \times 220 \times 85$ and $5 \times 11 \times 17$ grid cells, respectively.
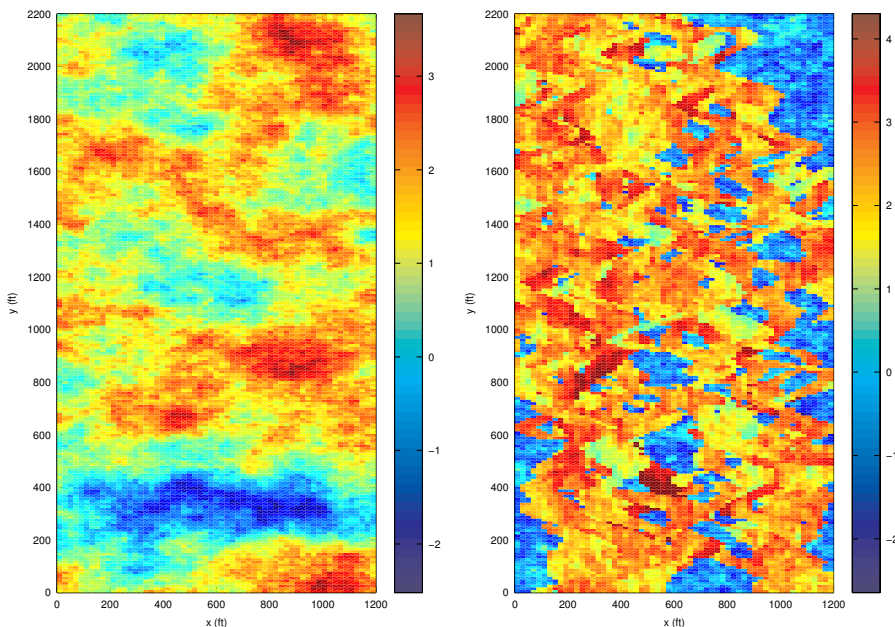

Fig. 4. Logarithm of horizontal permeability for layers in the Tarbert (left) and Upper Ness formations (right).

with a standard two-point flux-approximation. We also compare the MMs-FEM solutions with coarse-grid solutions obtained by a standard upscaling method [20] and with fine-grid solutions obtained with the upscaling-based, nested-gridding method introduced by Gautier, Blunt, and Christie [2].

In the upscaling technique, an upscaled diagonal permeability tensor is generated on the coarse grid by a flow simulation with a constant pressure drop in one of the coordinate directions and no-flow boundary conditions in the

other coordinate directions. The pressure equation (3) is then solved on the coarse grid using a finite-volume scheme with two-point flux-approximation and permeabilities given by the upscaled grid-block permeability tensors. This upscaling is also applied as part of the nested-gridding method, but, in the nested-gridding method the permeability-mobility product $(K\lambda_t)$ is upscaled. The induced coarse-grid fluxes are then used to determine boundary conditions for local subgrid problems in order to obtain a mass conservative velocity field on the subgrid scale.

Since the nested-gridding method uses a coarse grid pressure solver to solve (3) and streamline simulation to solve for fluid transport, it may be viewed as an upscaling-based analogue to the proposed methodology and is hence a natural method to compare with. However, to make the comparison between our approach and the nested-gridding method as fair as possible, we use the same inter-grid transfer operator to map the coarse grid fluxes onto a fine grid velocity field for the nested-gridding method as we do for MMsFEM with local boundary conditions. Hence, instead of using constant velocity boundary conditions to recover the subgrid velocity field for the nested-gridding method, as in [2], we use boundary conditions that are obtained by multiplying ν_{ij} in (17) with ν_{ij}^0 defined by (19) with the corresponding constant flux that we obtain from the upscaled coarse grid solution.

6.1 Two quarter-five spots in two space dimensions

Before attacking the full three-dimensional SPE 10 reservoir model, we first consider two quarter-five spot problems in two spatial dimensions. The porosity and permeability data sets are extracted on a 60×60 grid from the top and bottom layers, respectively, of the SPE 10 model. This means that Dataset 1 is from the smooth Tarbert formation, whereas Dataset 2 is from the channelised Upper Ness formation.

To assess the overall resolution of the flow pattern, we measure L^1 errors in saturation values given by

$$e(S) = \|S - S_{\text{ref}}\|_1 / \|S_{\text{ref}}\|_1. \tag{34}$$

Table 1 reports errors measured with (34) for all four methods using varying upscaling factors on both data sets. We see that the general trend for both datasets is that MMsFEM with *global* boundary conditions is the most accurate method, followed by MMsFEM with *local* boundary conditions and then nested gridding and upscaling, in that order. We also observe that errors for all methods are larger for the second dataset. The reason is that the second dataset has much stronger heterogeneous structures and contains channelling systems that are difficult to model with upscaling-based reservoir simulation regimes.
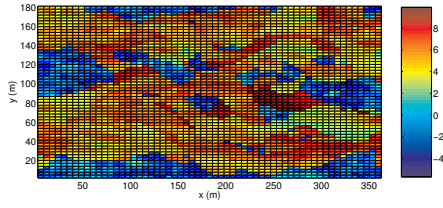
Table 1
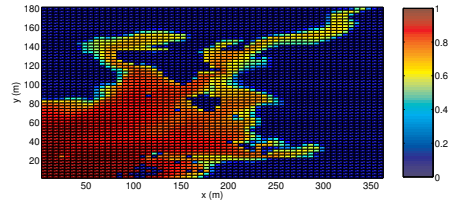Saturation field errors, $e(S)$, for Dataset 1 (top) and Dataset 2 (bottom).

Upsc. factor	Global BC	Local BC	Nested gridding	Upscaled
2×2	1.013e-02	1.094e-02	3.094e-02	6.801e-02
3×3	1.219e-02	1.732e-02	3.814e-02	1.005e-01
5×5	1.421e-02	2.889e-02	5.033e-02	1.497e-01
10×10	2.523e-02	5.377e-02	7.643e-02	2.415e-01
2×2	3.644e-02	4.132e-02	1.672e-01	2.383e-01
3×3	4.360e-02	6.705e-02	1.868e-01	2.864e-01
5×5	4.881e-02	9.659e-02	2.373e-01	3.812e-01
10×10	8.477e-02	1.981e-01	4.848e-01	7.217e-01

Figure 5 shows saturation profiles for Dataset 2 after an injection of water corresponding to 40% of the total pore volume in the reservoir. The grids are upscaled by a factor ten in each coordinate direction so that the coarse grid consists of only 6×6 blocks. The figure illustrates the improved resolution obtained by using subgrid information when solving the fluid transport. In particular, MMsFEM with global boundary conditions gives good resolution of both the global flow pattern and the local fingering due to high-permeable channels. MMsFEM with local boundary conditions resolves the global flow pattern accurately, but misses some of the finer details along the x-axis. Nested gridding is able to predict two of the major fingers, but over-predicts the flow close to the x-axis. The upscaled simulation, on the other hand, has lost all fine-scale information and only gives a crude approximation to the global flow pattern.
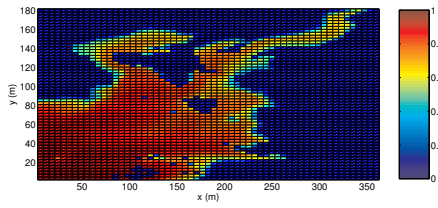
Not surprisingly, the results in this section shows that there is a clear benefit, as far as computational accuracy goes, in incorporating as much information as possible into the boundary conditions for the base functions. Moreover, even though nested gridding and MMsFEM with local boundary conditions use the same inter-grid transfer operator to map the coarse grid fluxes onto the subgrid velocity field, we see that MMsFEM performs consistently better than nested gridding. This is to be expected since MMsFEM is defined so that the coarse grid fluxes are coupled with the inter-grid transfer operator in a mathematically rigorous way, whereas the two operators are completely decoupled in the nested-gridding method.
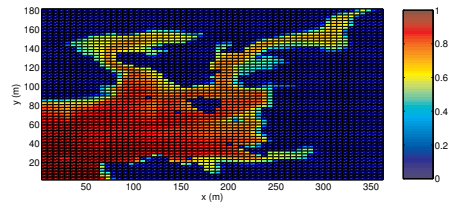
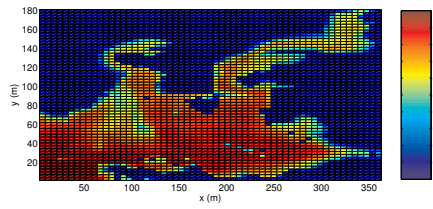(a) Horizontal permeability (log-arithm)
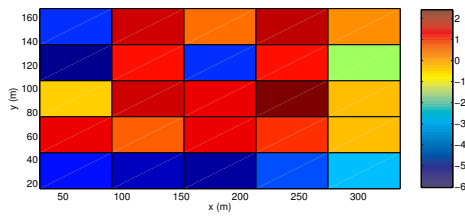

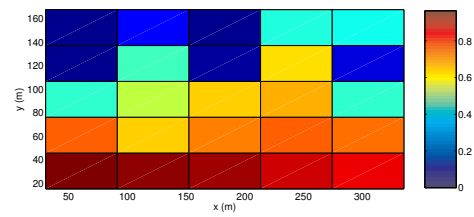(b) Reference solution

(c) Global BC

(d) Local BC

(e) Nested gridding

(f) Upscaled permeability (loga-rithm)

(g) Upscaled solution

Fig. 5. Permeabilities and water saturations near breakthrough time (0.4 PVI) for Dataset 2. The upscaling factor is 10×10 for all methods.
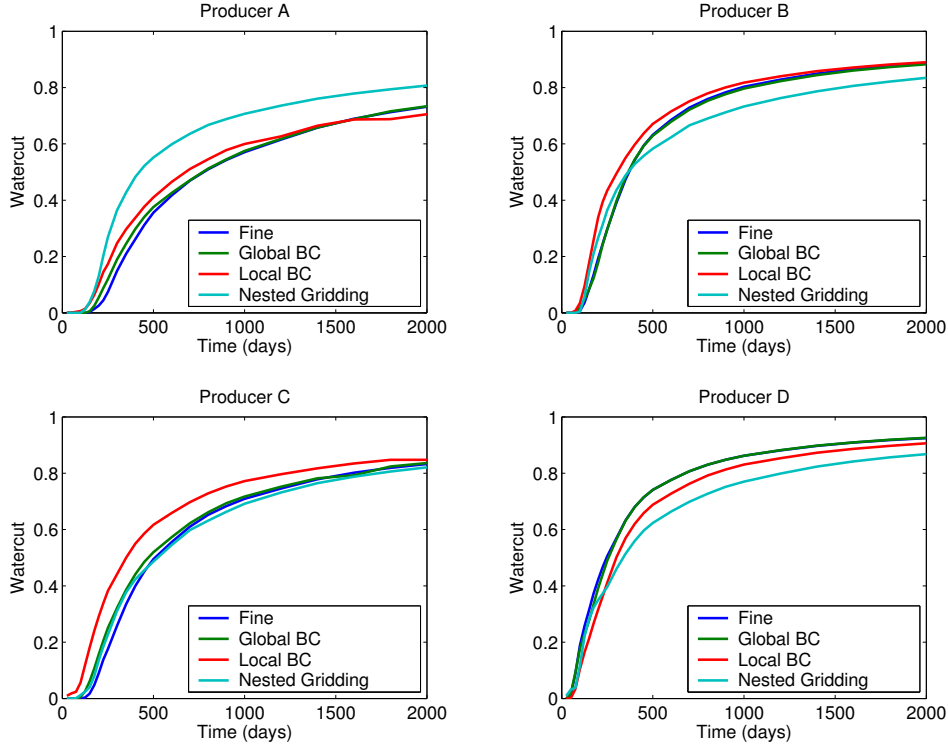
23

Fig. 6. Watercut curves for the full three dimensional SPE 10 model.

6.2 Tenth SPE comparative solution project: Model 2

We now demonstrate the performance of MMsFEM on the full SPE benchmark model. Figure 6 shows the water-cut curves $w_{wc}(t)$ for 2000 days of production simulated by nested gridding and by MMsFEM with local and global boundary conditions. In all simulations we used the time steps reported by StreamSim in [12]; that is, 25 days up to day 250, 50 days up to day 500, 100 days up to day 1000, and then 200 days.

The performance of MMsFEM with global boundary conditions is remarkably good; for all four producers the water-cut curves almost match the reference solution. This observation is confirmed by Table 2, which shows the relative L^1 errors of the water-cut curves defined as

$$e(w_{wc}) = \int |w_{wc}(t) - w_{wc}^{ref}(t)| \, dt / \int |w_{wc}^{ref}(t)| \, dt. \tag{35}$$

Here w_{wc}^{ref} are the respective water-cut curves induced by the reference solution. We see that the measured discrepancy between w_{wc}^{ref} and the water-cut curves produced by MMsFEM with global boundary conditions is only a few percent for each producer. Such an accuracy can hardly be achieved on this difficult dataset with any traditional upscaling method, particularly not with an upscaling factor as large as $10 \times 22 \times 5$. We also want to emphasise that the

24

Table 2
Relative errors of the water-cut curves for the SPE case.

	Global BC	Local BC	Nested gridding
Producer A	4.358e-02	1.390e-01	3.917e-01
Producer B	1.147e-02	1.025e-01	9.895e-02
Producer C	6.635e-02	2.611e-01	5.302e-02
Producer D	1.437e-02	9.350e-02	1.354e-01
Average	3.395e-02	1.491e-01	1.698e-01

results involved *no tuning* of parameters, except for choosing the time steps and the coarse grid. In fact, our only criteria was to have the fine-grid as a natural subgrid of the coarse grid, and to have a sufficiently small coarse grid to reduce the time spent on linear algebra.

The results in Table 2 also show that, on average, MMsFEM with local boundary conditions gives better results than the nested-gridding method, even though the nested-gridding method gives the most accurate water-cut curve of all three methods on Producer C.

7 Concluding Remarks

We have presented a novel method for accurate resolution of both global and local flow patterns in large heterogeneous geomodels. The approach is based on a combination of a multiscale discretisation method for the pressure equation and a standard streamline method for the fluid transport equation. In the multiscale method, the pressure is computed on a coarsened grid using numerically constructed approximation spaces that incorporate the local heterogeneities of the elliptic operator on the underlying fine grid. Given the high efficiency of the streamline method, the fluid transport equation is solved directly on the fine grid using Darcy velocities obtained by utilising the subgrid structures in the mixed FEM base functions that span the approximation space for the Darcy velocity. Although gravity was not explicitly treated in the numerical examples, it is well within the capabilities of the current methodology.

The key to obtain accurate subgrid velocity fields lies in the specification of proper boundary conditions for the base functions. We have considered a local approach, in which the boundary conditions reflect the local heterogeneous structures and accounts for a radial flow pattern in the proximity of wells, and a global approach where the boundary conditions are determined from the initial velocity field on the fine grid. The multiscale approaches have been compared with both coarse grid simulations using a standard upscal-

ing technique and a nested-gridding method that solves the pressure equation on a coarse grid and the saturation equation on the fine grid using streamlines. The latter method serves as a natural upscaling-based counterpart of our multiscale method with local boundary conditions.

The results show that the multiscale simulation method with global boundary conditions is the most accurate and robust method. The results also show that the corresponding multiscale method with local boundary conditions performs, on average, better than the nested-gridding method. This trend has also been verified on another three dimensional test case in [1], and in other simulations conducted by the authors. The results therefore supports our claim that multiscale methods combined with streamlines can give improved accuracy, and may become a robust and efficient alternative to traditional upscaling approaches. In fact, we believe that this multiscale approach can lay the ground for direct simulation of large, high-resolution geomodels obtained from reservoir characterisation.

In this paper we have only briefly touched upon the great flexibility of multiscale finite-element methods, which is their second, and maybe most important advantage. Since the base functions are constructed numerically, they are not restricted to polygonal elements as is the case for ordinary finite elements and conventional finite-volume methods. Indeed, multiscale base functions can, at least in principle, be constructed on coarse blocks of arbitrary shape. This gives an enormous flexibility in handling complex grids as specified by geologists to model natural rock phenomena like faults, eroded cells, etc. However, how well the multiscale approach performs on unstructured and largely irregular grids is still unsettled and is an interesting topic for further research. Preliminary results show that the methodology performs well on irregular corner-point grids without faults or throws.

We also believe that it is possible to extend the methodology to mildly compressible flows and to multicomponent or three-phase flows. For three-phase flow, the interesting question is how the tighter coupling between the pressure and the fluid transport equations affects the dynamical behaviour of the local basis functions. In particular, the strong coupling between the pressure equation and the phase transport equations may imply that one needs to update the base functions more often. Hence, an issue that should be given further attention is the use of adaptive strategies to speed up multi-phase flow simulations. This includes regenerating base functions only in regions where the total mobility has changed significantly, and exploiting the information in the multiscale base functions to construct efficient adaptive numerical schemes for the phase transport equation.

Finally, we have not discussed the numerical linear algebra in great detail, a topic which is of great importance if we want to apply the proposed methodology to large real-field geomodels. This topic is part of ongoing research.

References

[1] J. E. Aarnes, On the use of a mixed multiscale finite element method for greater flexibility and increased speed or improved accuracy in reservoir simulation, Multiscale Model. Simul. 2 (3) (2004) 421–439.

[2] Y. Gautier, M. J. Blunt, M. A. Christie, Nested gridding and streamline-based simulation for fast reservoir performance prediction, Comp. Geosci. 3 (1999) 295–320.

[3] M. Crane, F. Bratvedt, K. Bratvedt, P. Childs, R. Olufsen, A fully compositional streamline simulator, in: SPE Annual Technical Conference and Exhibition, SPE 63156, Dallas, Texas, 2000.

[4] M. R. Thiele, R. P. Batycky, M. J. Blunt, A streamline-based 3D field scale compositional reservoir simulator, in: SPE Annual Technical Conference and Exhibition, SPE 38889, San Antonio, Texas, 1997.

[5] I. Aavatsmark, T. Barkve, Ø. Bøe, T. Mannseth, Discretization on unstructured grids for inhomogeneous, anisotropic media. part i: Derivation of the methods, Siam J. Sci. Comp. 19 (5) (1998) 1700–1716.

[6] I. Aavatsmark, T. Barkve, Ø. Bøe, T. Mannseth, Discretization on unstructured grids for inhomogeneous, anisotropic media. part ii: Discussion and numerical results, Siam J. Sci. Comp. 19 (5) (1998) 1717–1736.

[7] M. Edwards, R. Lazarov, I. Y. (eds.), Special issue on locally conservative numerical methods for flows in porous media, Comp. Geosci. 6 (3-4) (2002) 225–579.

[8] T. Hou, X.-H. Wu, A multiscale finite element method for elliptic problems in composite materials and porous media, J. Comput. Phys. 134 (1997) 169–189.

[9] Z. Chen, T. Hou, A mixed multiscale finite element method for elliptic problems with oscillating coefficients, Math. Comp. 72 (2003) 541–576.

[10] P. Jenny, S. H. Lee, H. A. Tchelepi, Multi-scale finite-volume method for elliptic problems in subsurface flow simulation, J. Comput. Phys. 187 (2003) 47–67.

[11] T. Arbogast, An overview of subgrid upscaling for elliptic problems in mixed form, in: Z. Chen, R. Glowinski, K. Li (Eds.), Current trends in scientific computing, Contemporary Mathematics, AMS, 2003, pp. 21–32.

[12] M. A. Christie, M. J. Blunt, Tenth SPE comparative solution project: A comparison of upscaling techniques, SPE Reservoir Engineering and Evaluation 4 (4) (2001) 308–317.

[13] F. Bratvedt, T. Gimse, C. Tegnander, Streamline computation for porous media flow including gravity, Transp. Porous Media (1996) 62–78.

[14] D. Pollock, Semianalytical computation of path lines for finite difference models, Ground Water 26 (1988) 743–750.

[15] M. Prévost, M. G. Edwards, M. J. Blunt, Streamline tracing on curvilinear structured and unstructured grids, SPE Journal 7 (2) (2002) 139–148.

[16] H. Holden, N. H. Risebro, Front Tracking for Hyperbolic Conservation Laws, Springer, New York, 2002.

[17] D. Peaceman, Interpretation of well-block pressures in numerical reservoir simulation with nonsquare grid blocks and anisotropic permeability, Society of Pet. Eng. Journal (1983) 531–543.

[18] Y. Saad, Iterative methods for sparse linear systems, PWS Publishing Co., Boston, 1996.

[19] J. Bramble, J. Pasciak, A. Vassilev, Analysis of the inexact uzawa algorithm for saddle point problems, SIAM Numer. Anal. 34 (1997) 1072–1092.

[20] L. J. Durlofsky, Numerical calculations of equivalent gridblock permeability tensors for heterogeneous porous media, Water Resour. Res. 27 (5) (1991) 699–708.